Electronic Supplementary Material (ESI) for Journal of Materials Chemistry A.
This journal is © The Royal Society of Chemistry 2021

Supplementary Information

Defect-rich N-doped CeO_2 supported by N-doped graphene as a metal-free plasmonic hydrogen evolution photocatalyst

Apparent quantum yield efficiency calculation:

The apparent quantum yield (AQY) efficiency for HER activity have been performed to understand the effect of the different irradiation wavelengths over the photocatalytic performance of nanocomposite materials. The AQY efficiency, thereby, are calculated based on the amount of hydrogen evolution in the duration t of a single incident wavelength exposure using the following equation:

$$AQY\ efficiency\ [\%] = \frac{Numbers\ of\ evoluted\ hydrogen\ molecules\ x\ 2}{Number\ of\ incident\ photons}\ x\ 100$$

$$Number\ of\ incident\ photons = \frac{E_{total}}{E_{photon}} = \frac{PS\lambda_{inc}t}{hc}$$

Finally, the AQY efficiency is calculated by:

$$AQY\ efficiency\ (\%) = \frac{2n_{H_2,t}N_A hc}{PS\lambda_{inc}t}x\ 100$$

Where, $n_{H_2,t}$ (mol) represents the amount of hydrogen evolution in the duration time (t) of incident monochromatic light exposure, λ_{inc} (m); N_A (mol^{-1}) is Avogadro's constant; h (J s) is Planck's constant, c ($m\ s^{-1}$) is the speed of light; P ($W\ m^{-2}$) presents the power density of the incident monochromatic light; and S (m^2) is the irradiation area. The incident light wavelength is controlled by a 300 W xenon lamp (Asahi, Max 303) with an appropriate band pass filter inserted between light source and made reactor.

Table S1. Free energy corrections calculated for H_2 molecule and H* adsorbate. All values are in eV.

	ZPE	$\int C_p dT$	$-T\Delta S$
H_2 (g)	0.267	0.091	-0.554
H*	0.023	0.009	-0.014

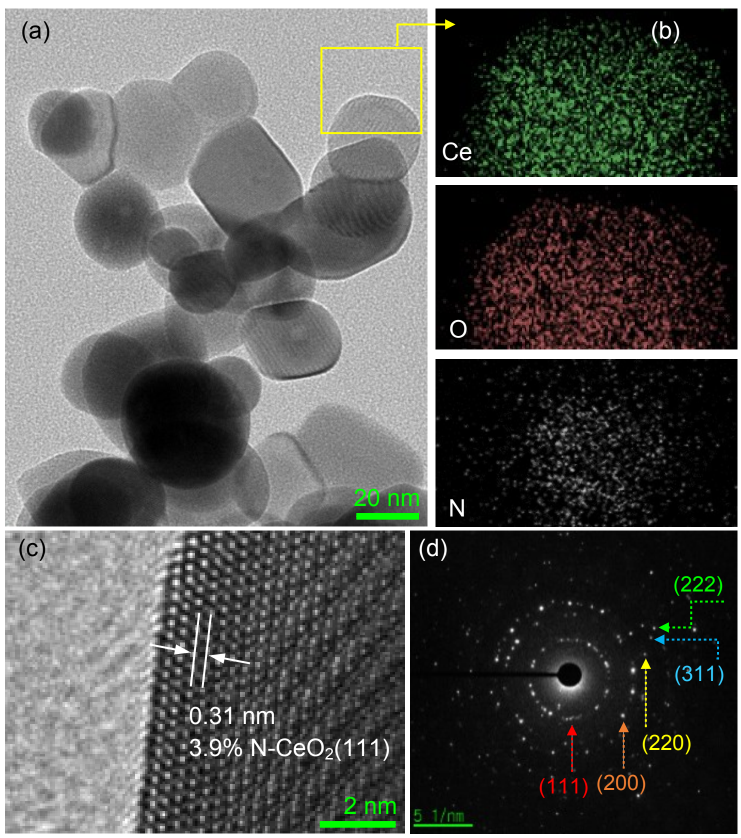

Fig. S1 (a) TEM observation, (b) EDS elemental mapping of as-pyrolyzed 3.9% N-CeO_2 nanoparticles, (c) high-resolution TEM image of 3.9% N-CeO_2 with lattice fringe of (111) plane, and (d) SAED pattern of assembly 3.9% N-CeO_2 nanoparticle.

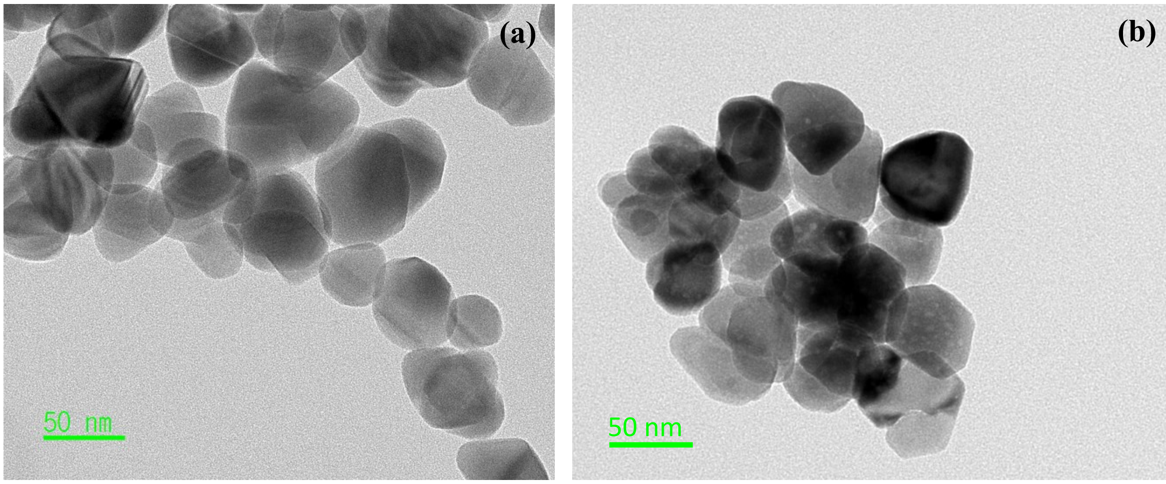

Fig. S2 (a, b) TEM observation of as-pyrolyzed 1.8 and 7.6% N-CeO_2 NPs.

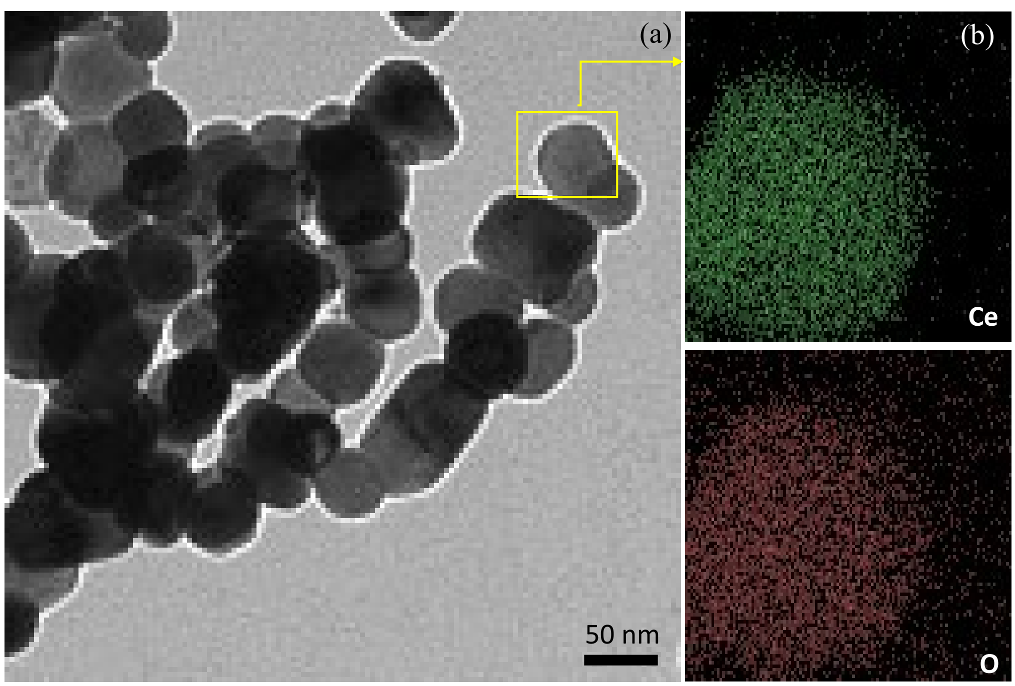

Fig. S3 (a) TEM observation and (b) TEM elemental mapping of as-pyrolyzed undoped CeO_2.

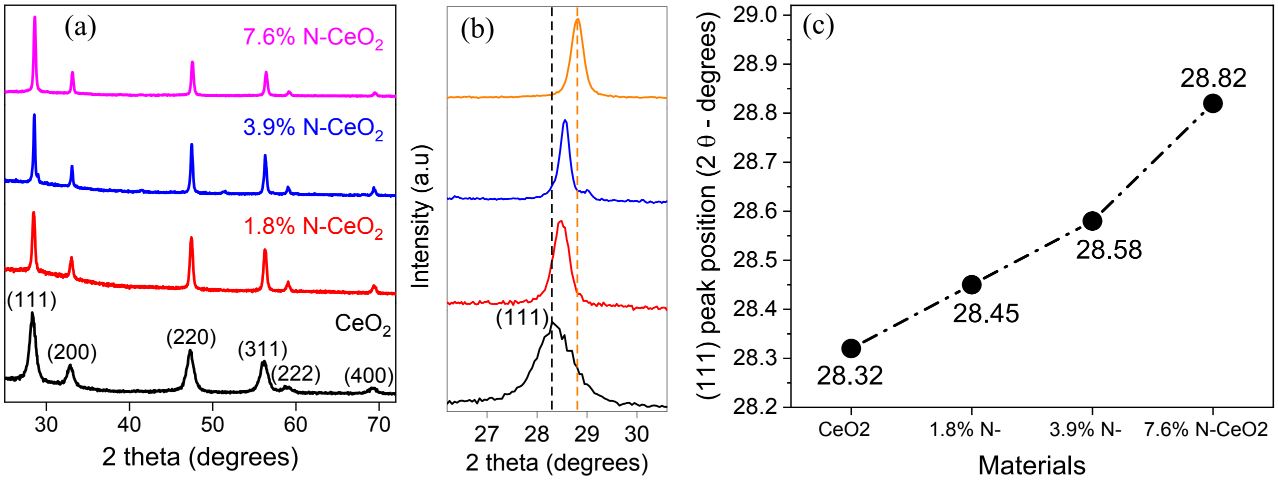

Fig. S4 (a) XRD analysis for as-pyrolyzed undoped CeO_2, 1.8 % N-CeO_2, 3.9% N-CeO_2, and 7.6% N-CeO_2 nanocomposites. (b, c) Corresponding change in (111) peak positions.

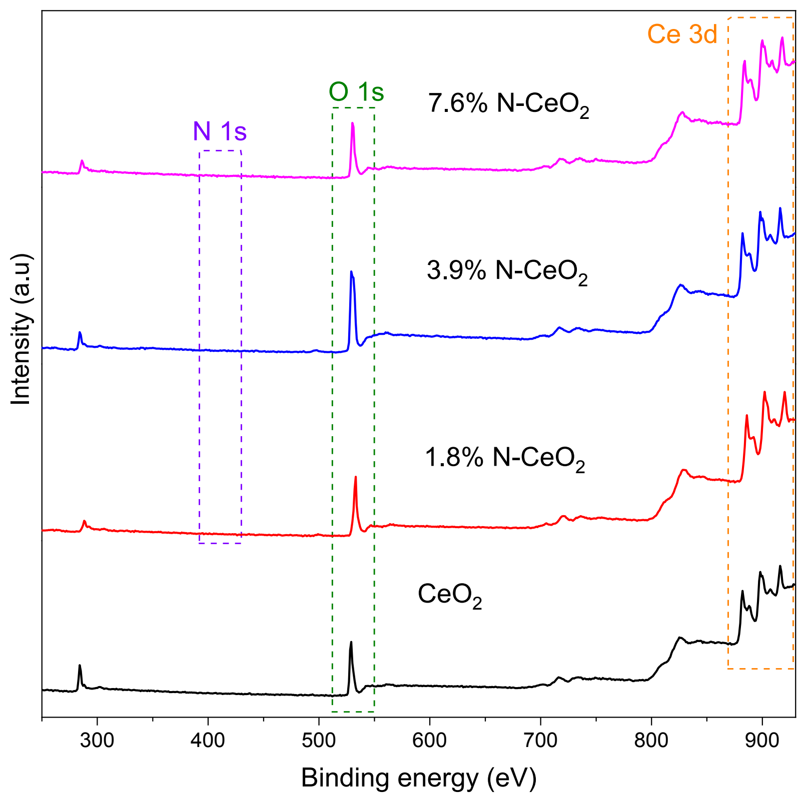

Fig. S5 Full XPS survey measured by prolonging the integration time to carefully detect the chemical compositions of as-pyrolyzed undoped CeO_2, 1.8% N-CeO_2, 3.9% N-CeO_2, and 7.6% N-CeO_2 nanocomposites.

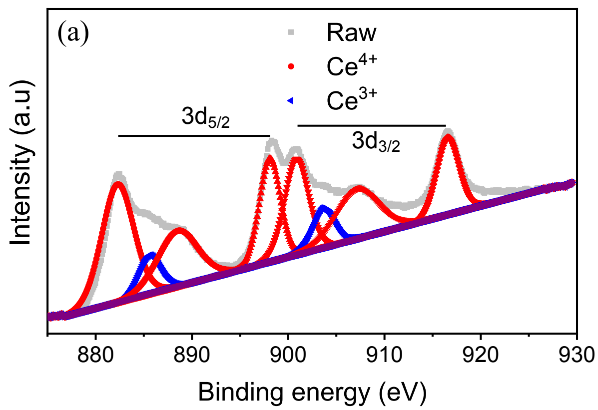

Fig. S6 High-resolution XPS analysis of (a) Ce 3d and (b) O 1s for as-pyrolyzed undoped CeO_2.

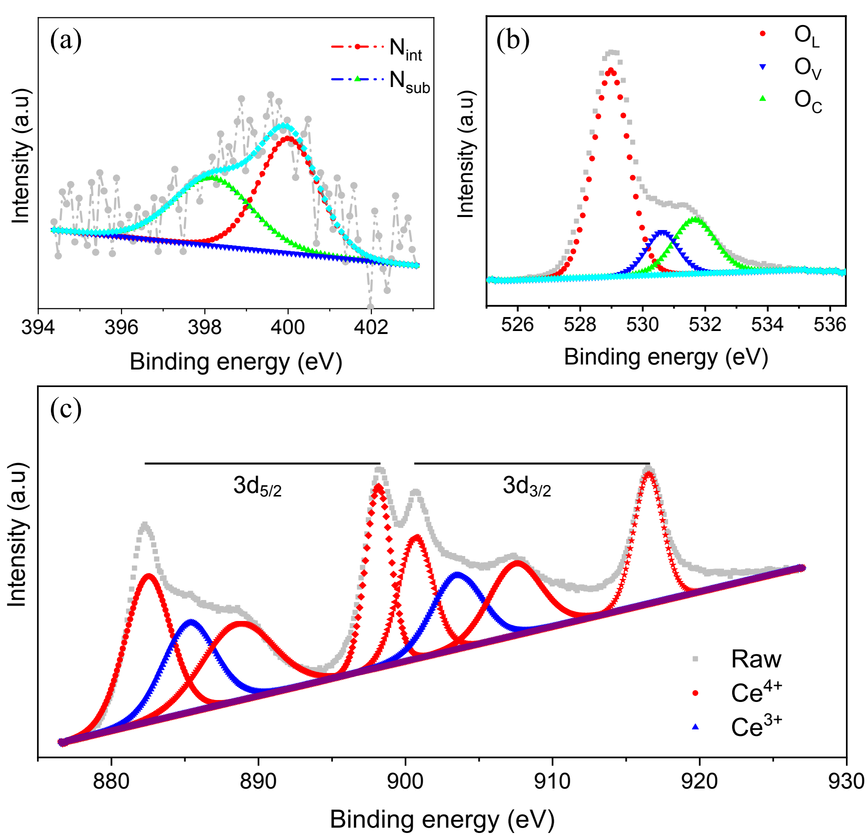

Fig. S7 High-resolution XPS analysis of (a) N 1s, (b) O 1s, and (c) Ce 3d for as-pyrolyzed 3.9% N-CeO_2.

Table S2. XPS fitting result comparison for as-calcined undoped CeO_2 and N-doped CeO_2, and 3.9% N-CeO_2/N-Gr samples.

Samples	**Ce^{3+}**		**Oxygen**		
	Binding energy (eV)	Relative percentage (%)	Species	Binding energy (eV)	Relative percentage (%)
CeO_2	884.83 903.02	**13.11**	O_L (Ce-O)	528.97	64.57
			O_V (vacancy)	**530.32**	**13.59**
			O_C (chemisorbed)	531.95	21.84
1.8% N-CeO_2	885.84 903.10	**15.32**	O_L (Ce-O)	529.15	63.89
			O_V (vacancy)	530.32	15.86
			O_C (chemisorbed)	532.03	20.25
3.9% N-CeO_2	885.05 903.16	**22.47**	O_L (Ce-O)	529.34	58.92
			O_V (vacancy)	**530.45**	**19.52**
			O_C (chemisorbed)	532.07	21.56
7.6% N-CeO_2	885.29 903.52	**24.92**	O_L (Ce-O)	529.52	50.17
			O_V (vacancy)	530.73	23.56
			O_C (chemisorbed)	532.35	26.27
3.9% N-CeO_2/N-Gr	885.31 903.47	**23.08**	O_L (Ce-O)	529.53	51.12
			O_V (vacancy)	**530.84**	**20.17**
			O_C (chemisorbed)	532.41	27.71

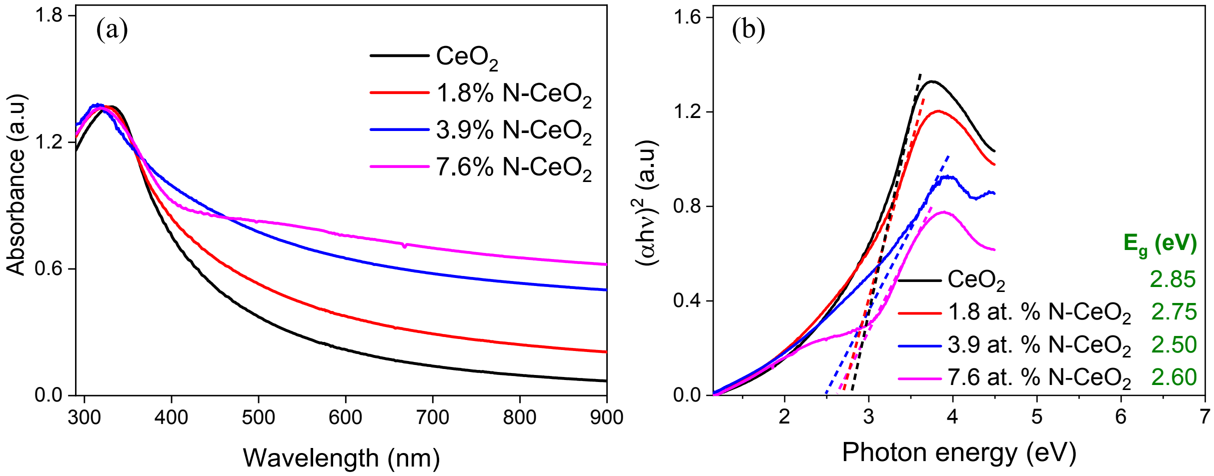

Fig. S8 (a) UV-vis absorption spectra of as-calcined CeO_2 and N-CeO_2 materials and (b) plot of $(\alpha h\nu)^2$ vs. photon energy with estimated bandgap energy (E_g) measured by Tauc's equation.

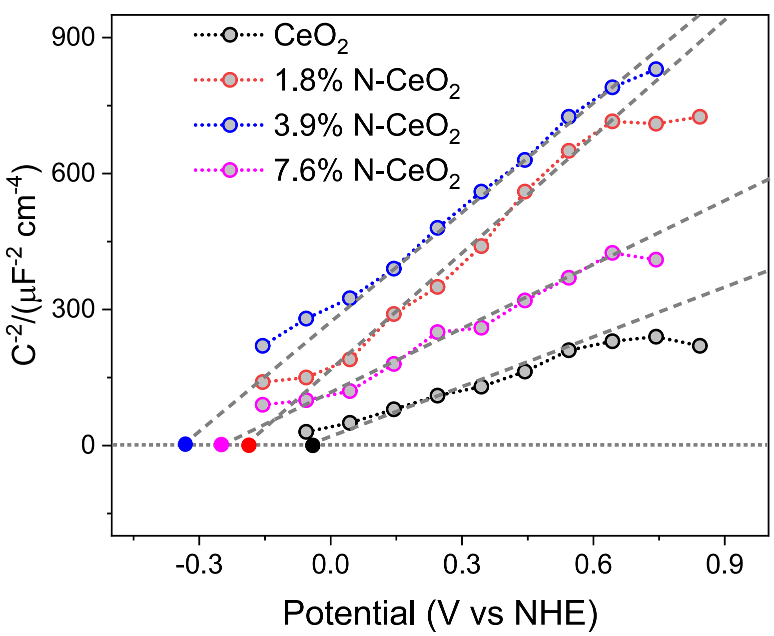

Fig. S9 Mott-Schottky plots based on impedance measurement at frequency of 20 kHz for as-calcined CeO_2 and N-CeO_2.

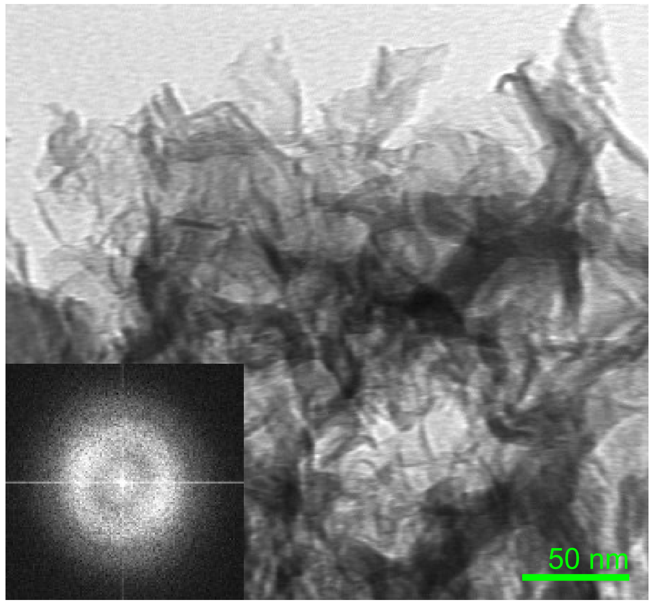

Fig. S10 TEM observation of as-pyrolyzed free N-Gr.

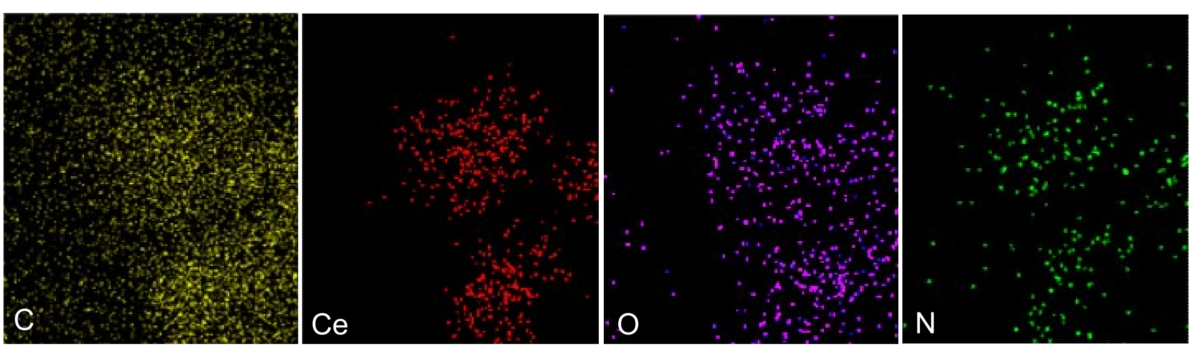

Fig. S11 EDS elemental mapping for as-pyrolyzed 3.9% N-CeO_2/N-Gr nanocomposites.

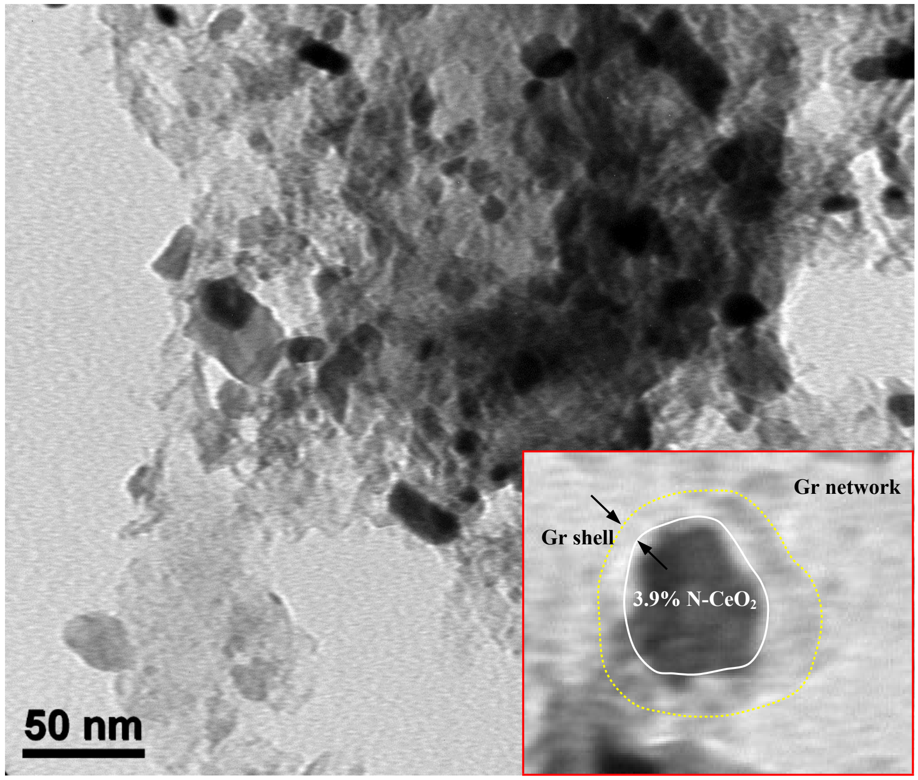

Fig. S12 TEM analysis for as-pyrolyzed 3.9% N-CeO_2/Gr nanocomposites.

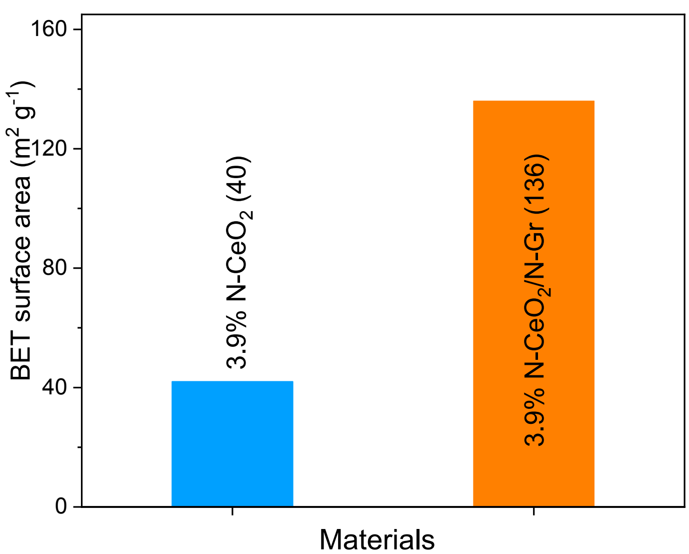

Fig. S13 Corresponding BET surface area for as-pyrolyzed 3.9% N-CeO_2 and 3.9% N-CeO_2/N-Gr photocatalysts.

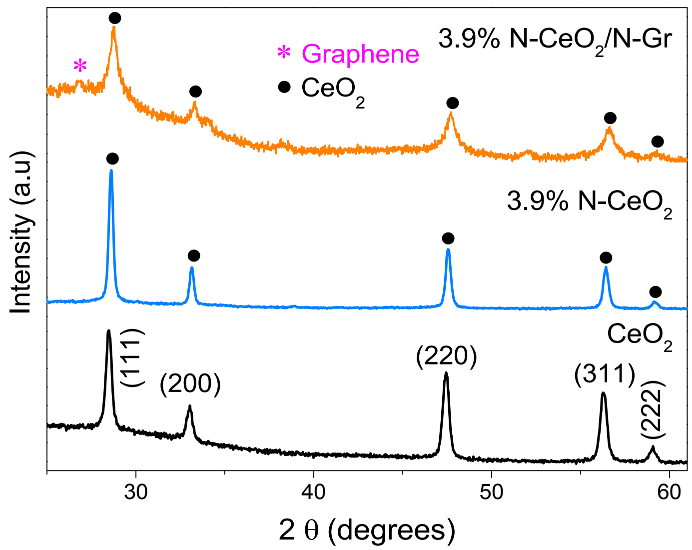

Fig. S14 XRD analysis for as-pyrolyzed undoped CeO_2, 3.9% N-CeO_2, and 3.9% N-CeO_2/N-Gr nanocomposites.

In case of 3.9% N-CeO_2/N-Gr (yellow), ceria XRD peaks are highlighted with (•). The XRD pattern of 3.9% N-CeO_2/N-Gr nanocomposites further consists of a small diffraction peak at around 26°, which corresponds to nitrogen-doped graphene, as marked with (*).

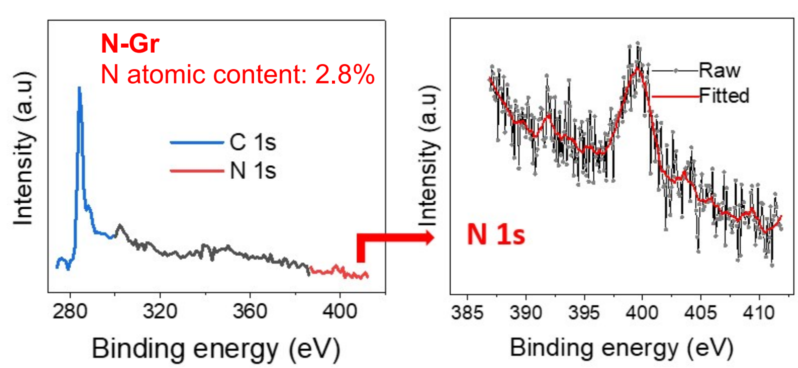

Fig. S15 Full XPS investigation of as-prepared N-Gr and high-resolution XPS analysis of N 1s.

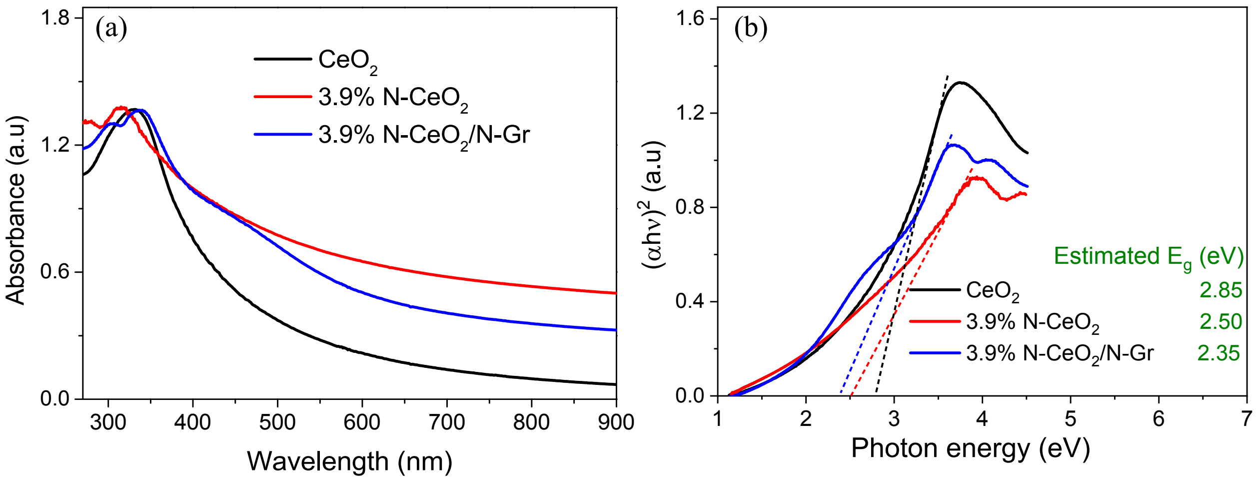

Fig. S16 (a) UV-vis absorption spectra and (b) corresponding plot of $(\alpha h\nu)^2$ vs. photon energy of as-pyrolyzed undoped CeO_2 and 3.9% N-CeO_2, and 3.9% N-CeO_2/N-Gr nanocomposites.

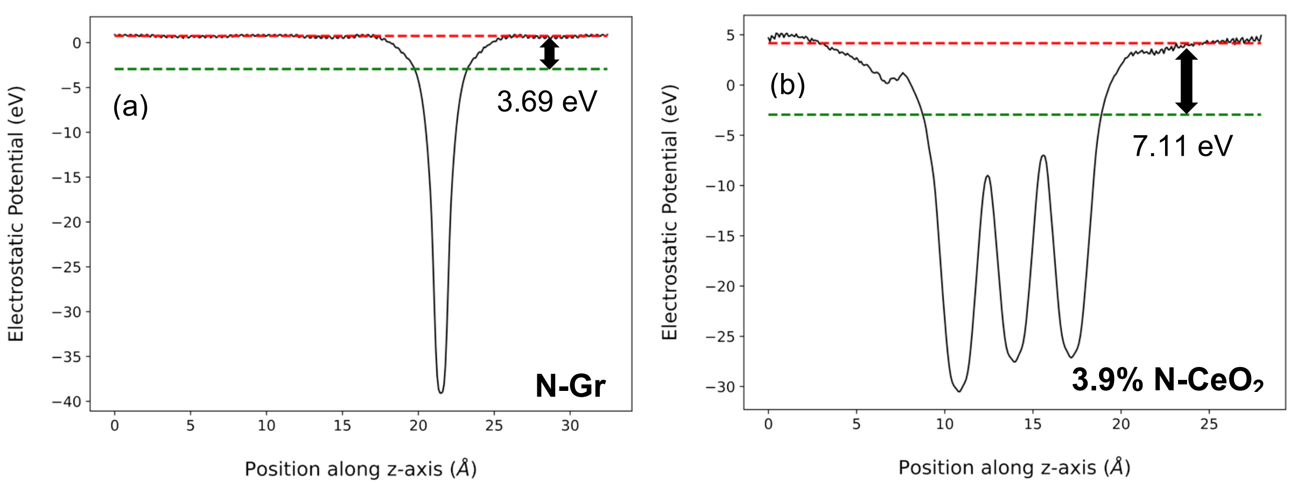

Fig. S17 The local electrostatic potential to calculate the work function values for (a) N-Gr and (b) 3.9% N-CeO_2 (111). Red and green horizontal dashed lines correspond to the vacuum level and the Fermi level, respectively.

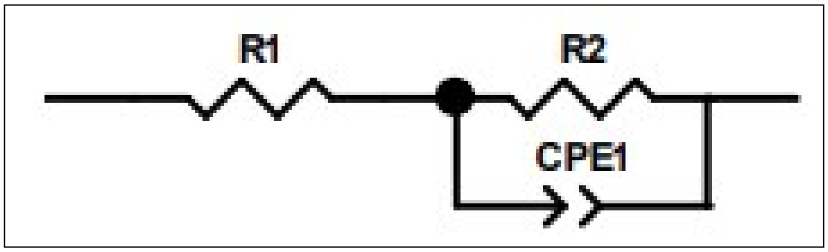

Fig. S18 A circuit used to fit the Nyquist plots: R1 is the solution resistance, R2 is the charge transfer resistance, and CPE1 is a constant phase element.[1]

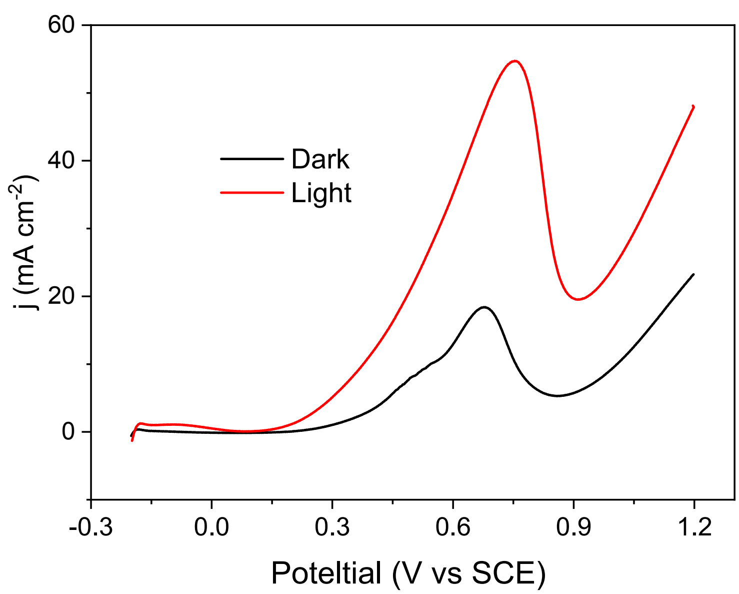

Fig. S19 MOR activity for 3.9% N-CeO_2/N-Gr nanocomposites with and without visible-light irradiation.

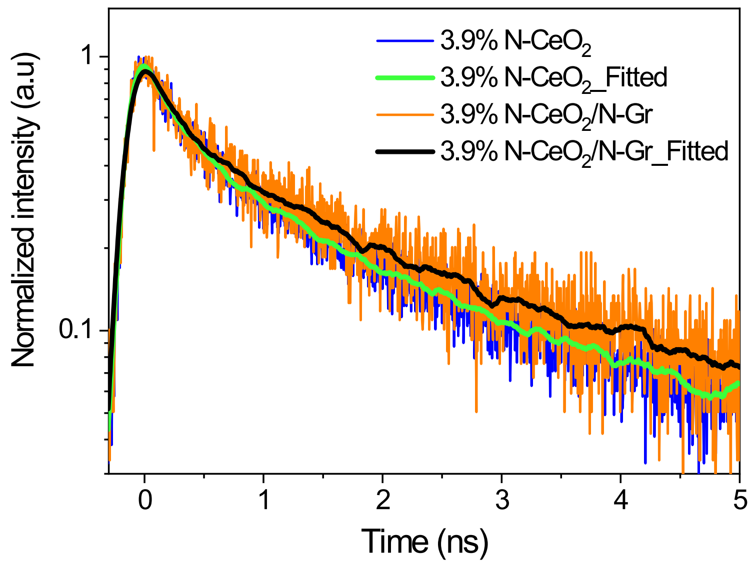

Fig. S20 Time-resolved photoluminescence (TRPL) spectra monitored at 500 nm for 3.9% N-CeO_2 and 3.9% N-CeO_2/N-Gr samples.

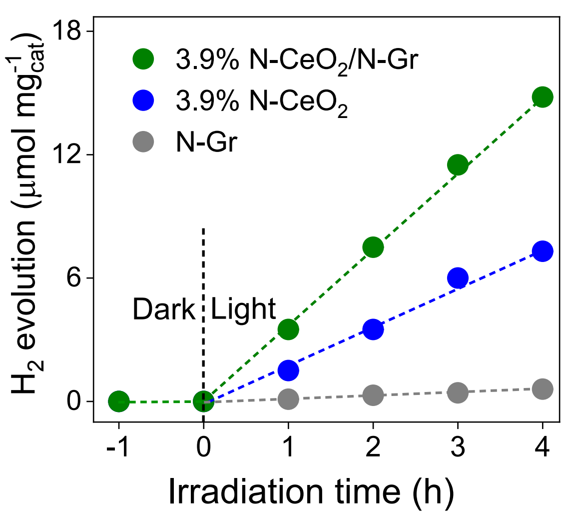

Fig. S21 Time-dependent photocatalytic hydrogen evolution amount for N-Gr, 3.9% N-CeO_2, and 3.9% N-CeO_2/N-Gr nanohybrids.

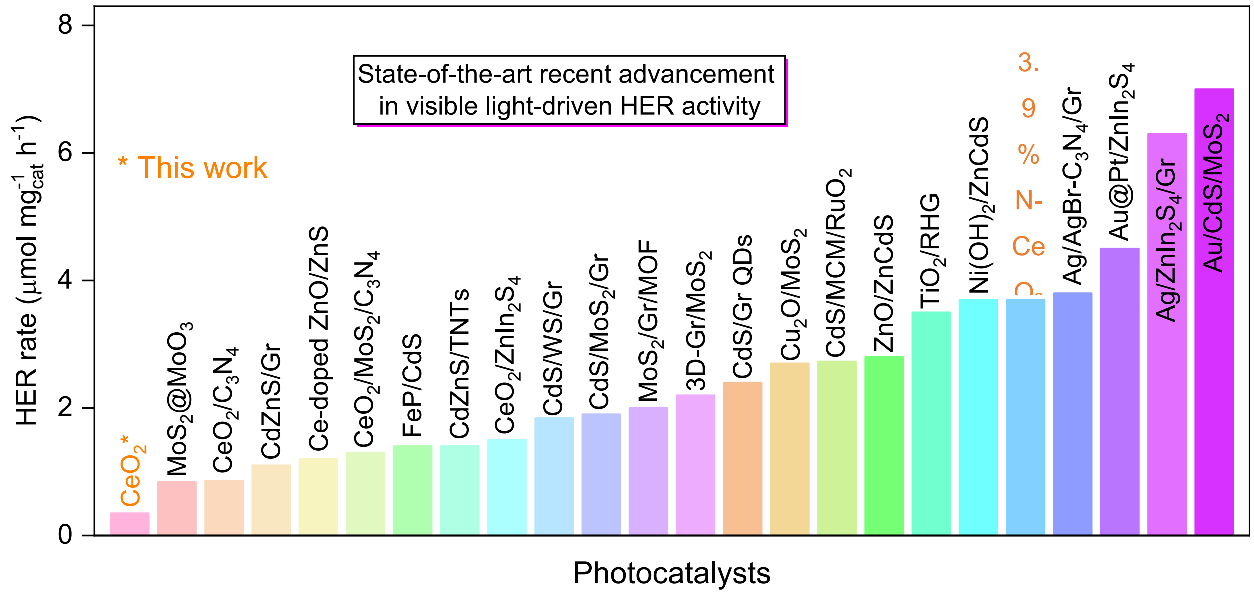

Fig. S22 A comparison of visible light-driven hydrogen evolution reactions based on current advanced photocatalysts reported in recent literatures.[2-24]

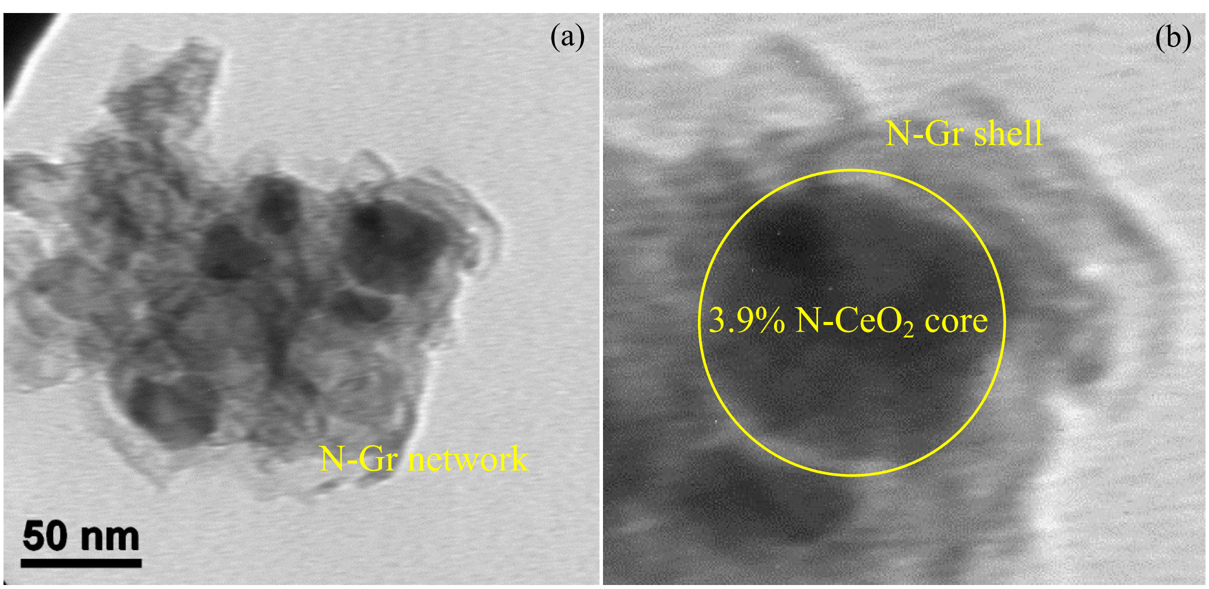

Fig. S23 TEM analysis for as-used 3.9% N-CeO$_2$/N-Gr nanocomposites after long-term HER stability test over 20 h.

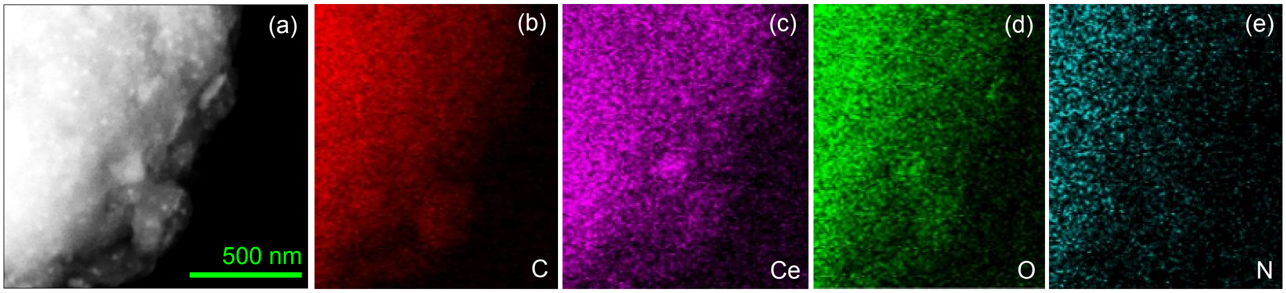

Fig. S24 (a) Field-emission SEM observation for as-used 3.9% N-CeO_2/N-Gr nanocomposites after stability test and (c-e) corresponding SEM-EDS elemental mapping.

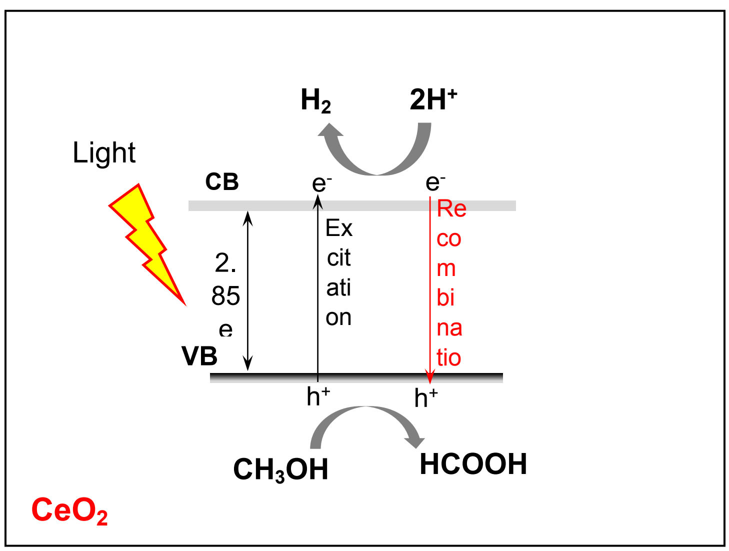

Fig. S25 Possible mechanism of HER over pure CeO_2 photocatalyst under visible-light irradiation.

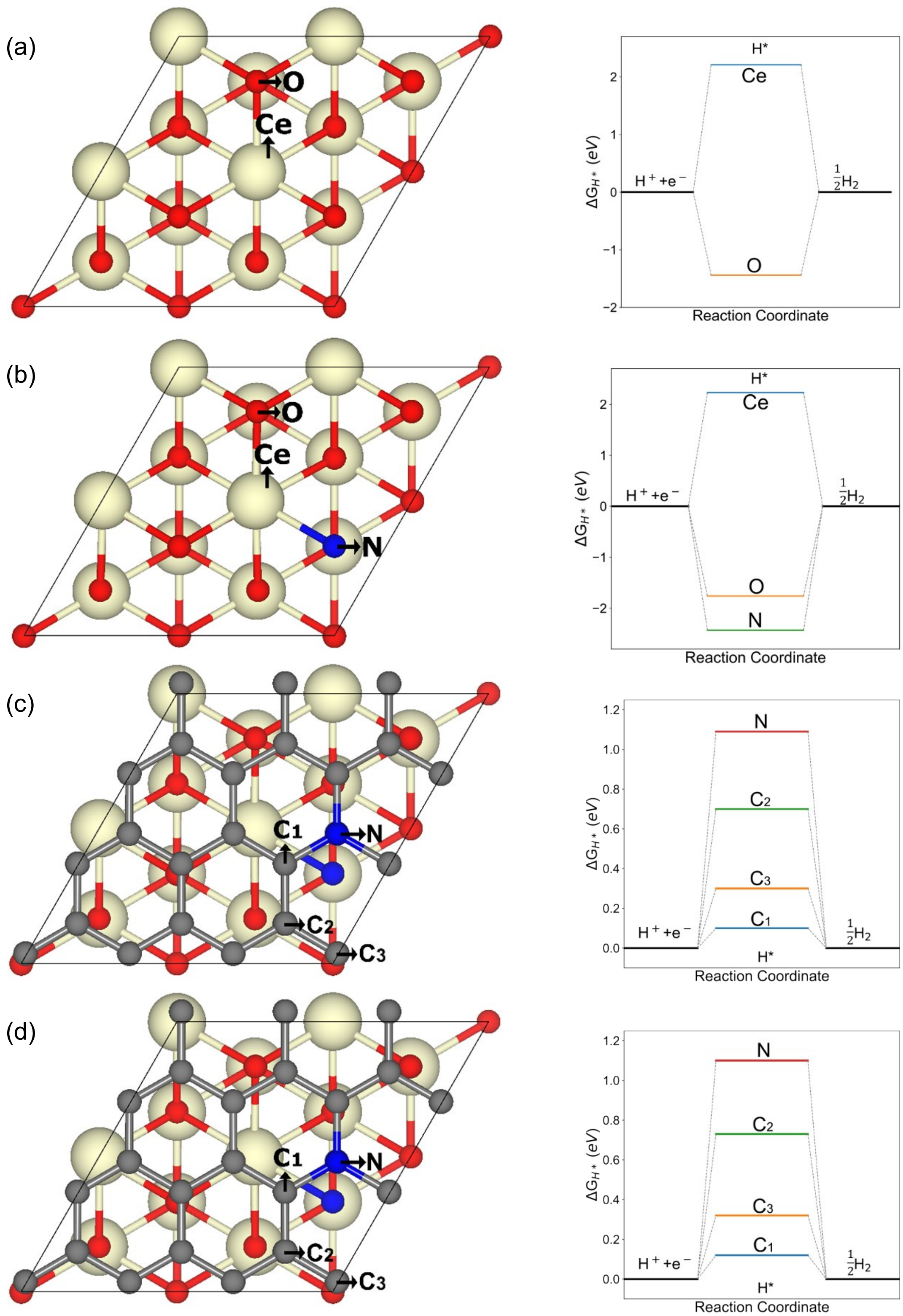

Fig. S26 Free energy diagram of (a) CeO_2, (b) 3.9% N-CeO_2, (c) 3.9% N-CeO_2/N-Gr (two graphene layers), (d) 3.9% N-CeO_2/N-Gr (three graphene layers) for HER activity.

References

1 D. V. Dao, T. D. Le, G. Adilbish, I.-H. Lee and Y.-T. Yu, *J. Mater. Chem. A*, 2019, **7**, 26996-27006.

2 S. Guo, X. Li, X. Ren, L. Yang, J. Zhu and B. Wei, 2018, **28**, 1802567.

3 W. Zou, Y. Shao, Y. Pu, Y. Luo, J. Sun, K. Ma, C. Tang, F. Gao and L. Dong, *Appl. Catal. B: Environ.*, 2017, **218**, 51-59.

4 D. Akyüz, R. M. Zunain Ayaz, S. Yılmaz, Ö. Uğuz, C. Sarıoğlu, F. Karaca, A. R. Özkaya and A. Koca, *Inter. J. Hydrog. Energy*, 2019, **44**, 18836-18847.

5 C.-J. Chang, K.-L. Huang, J.-K. Chen, K.-W. Chu and M.-H. Hsu, *J. Taiwan Inst. Chem. Eng.*, 2015, **55**, 82-89.

6 C. Zhu, Y. Wang, Z. Jiang, F. Xu, Q. Xian, C. Sun, Q. Tong, W. Zou, X. Duan and S. Wang, *Appl. Catal. B: Environ.*, 2019, **259**, 118072.

7 K. Sun, J. Shen, Y. Yang, H. Tang and C. Lei, *Appl. Surf. Sci.*, 2020, **505**, 144042.

8 Y. Chen and L. Guo, *J. Mater. Chem.*, 2012, **22**, 7507-7514.

9 C. Jiang, H. Wang, Y. Wang and H. Ji, *Appl. Catal. B: Environ.*, 2020, **277**, 119235.

10 Q. Xiang, F. Cheng and D. Lang, 2016, **9**, 996-1002.

11 X. Yu, R. Du, B. Li, Y. Zhang, H. Liu, J. Qu and X. An, *Appl. Catal. B: Environ.*, 2016, **182**, 504-512.

12 X. Hao, Z. Jin, H. Yang, G. Lu and Y. Bi, *Appl. Catal. B: Environ.*, 2017, **210**, 45-56.

13 X. Li, S. Guo, W. Li, X. Ren, J. Su, Q. Song, A. J. Sobrido and B. Wei, *Nano Energy*, 2019, **57**, 388-397.

14 Y. Lei, C. Yang, J. Hou, F. Wang, S. Min, X. Ma, Z. Jin, J. Xu, G. Lu and K.-W. Huang, *Appl. Catal. B: Environ.*, 2017, **216**, 59-69.

15 C. G. Morales-Guio, S. D. Tilley, H. Vrubel, M. Grätzel and X. Hu, *Nat. Commun.*, 2014, **5**, 3059.

16 R. Peng, C.-M. Wu, J. Baltrusaitis, N. M. Dimitrijevic, T. Rajh and R. T. Koodali, *Chem. Com.*, 2013, **49**, 3221-3223.

17 X. Wang, G. Liu, Z.-G. Chen, F. Li, G. Q. Lu and H.-M. Cheng, *J. Mater. Research*, 2010, **25**, 39-44.

18 U. Rajeena, M. Akbar, P. Raveendran and R. M. Ramakrishnan, *Inter. J. Hydrog. Energy*, 2020, **45**, 9564-9574.

19 W. Li, X. Wang, M. Li, S.-a. He, Q. Ma and X. Wang, *Appl. Catal. B: Environ.*, 2020, **268**, 118384.

20 Y. Xu, Y. Gong, H. Ren, W. Liu, C. Li, X. Liu and L. Niu, *J. Alloy. Compd.*, 2018, **735**, 2551-2557.

21 Y. Gao, B. Xu, M. Cherif, H. Yu, Q. Zhang, F. Vidal, X. Wang, F. Ding, Y. Sun, D. Ma, Y. Bi and Z. Xu, *Appl. Catal. B: Environ.*, 2020, **279**, 119403.

22 R. K. Chava, J. Y. Do and M. Kang, *ACS Sustain. Chem. Eng.*, 2018, **6**, 6445-6457.

23 B. Han, L. Wu, J. Li, X. Wang, Q. Peng, N. Wang and X. Li, *Inter. J. Hydrog. Energy*, 2020, **45**, 1559-1568.

24 H. An, Z. Lv, K. Zhang, C. Deng, H. Wang, Z. Xu, M. Wang and Z. Yin, *Appl. Surf. Sci.*, 2021, **536**, 147934.